THE JOURNAL OF BIOLOGICAL CHEMISTRY VOL. 287, NO. 17, pp. 13620–13632, April 20, 2012

Neutral Sphingomyelinase 2 Deficiency Increases Hyaluronan Synthesis by Up-regulation of Hyaluronan Synthase 2 through Decreased Ceramide Production and Activation of Akt*[S]

Received for publication, September 19, 2011, and in revised form, February 21, 2012 Published, JBC Papers in Press, March 1, 2012, DOI 10.1074/jbc.M111.304857

Jingdong Qin[‡], Evgeny Berdyshev[§], Christophe Poirer[¶], Nancy B. Schwartz[‡‖], and Glyn Dawson[‡‖1]

From the Departments of [‡]Pediatrics and [‖]Biochemistry and Molecular Biology, University of Chicago, Chicago, Illinois 60637, the [§]Department of Medicine, Institute for Personalized Respiratory Medicine, University of Illinois, Chicago, Illinois 60612, and the [¶]Georgia Health Sciences University, Vascular Biology Center, Athens, Georgia 30912

Background: Fibroblasts from the *fro*/*fro* mouse contained reduced amounts of ceramides and elevated amounts of hyaluronan (HA).
Results: Increased HA secretion was associated with increased activity of the Akt pathway and enhanced expression of the *HAS2* gene.
Conclusion: HA synthesis is regulated by NSMase2/ceramide through ceramide-activated phosphatase PP2A and Akt signaling pathway.
Significance: There is a direct link between sphingolipid and glycosaminoglycan metabolism.

Fibroblasts from the *fro*/*fro* mouse, with a deletion in the *Smpd3* gene coding for the active site of neutral sphingomyelinase 2 (NSMase2), secreted increased amounts of hyaluronan (HA). This was reversed by transfection with the *Smpd3* gene, suggesting a connection between sphingolipid and glycosaminoglycan metabolism. The deficiency of NSMase2 resulted in storage of sphingomyelin (SM) and cholesterol with a 50% reduction in ceramides (Cer). RT-PCR and Western blot analysis showed that increased HA secretion resulted from increased hyaluronan synthase 2 (HAS2) activity localized to sphingolipid-enriched lipid rafts. Although cholesterol levels were also elevated in lipid rafts from mouse fibroblasts deficient in lysosomal acid SMase activity (deletion of the *Smpd1*$^{-/-}$ gene), there was no increase in HA secretion. We then showed that in *fro*/*fro* fibroblasts, the reduced ceramide was associated with decreased phosphorylation of protein phosphatase 2A (PP2A) and increased phosphorylation of its substrate Akt-p, together with PI3K, PDK1, mTOR (mammalian target of rapamycin), and p70S6K, although PTEN was unaffected. Exogenous ceramide, as well as inhibitors of Akt (Akt inhibitor VIII), PI 3-kinase (LY294002 and wortmannin), and mTOR (rapamycin) reduced secretion of HA, whereas the NSMase2 inhibitor GW4869 increased HA synthesis and secretion. We propose that NSMase2/Cer are the key mediators of the regulation of HA synthesis, via microdomains and the Akt/mTOR pathway.

Osteogenesis imperfecta (OI)[2] is known as "brittle bone disease" and is commonly classified into eight types. The majority of cases (type I–IV) are caused by mutations in the genes encoding type 1 collagen (COL1A1 or COL1A2) (1). Others (types V–VIII) are noncollagenous forms, which are caused by mutation of the cartilage-associated protein (*Crtap*) gene, the *Lepre1* gene, and other unidentified genes and factors (2–4). Multiple mouse models for collagenous OI arose spontaneously or have been generated by transgenic techniques. The fragilitas ossium (*fro*) mouse with a spontaneous deletion in the gene *Smpd3* (encoding the active site of NSMase2) is the first mouse model representing noncollagenous OI, displays profound skeletal dysplasia pathologically consistent with OI, and suggests a vital role of NSMase2 in development (5–7).

NSMase2 is one of the major intracellular regulators of sphingolipids and many studies have implicated the activation of NSMase2 in ceramide-mediated signaling pathways that typically result in cell death (8–13). The level of expression of the gene encoding NSMase2 (*Smpd3*) is highest in brain and bone, with lesser expression in skin, sternum, and trachea and very little in heart, kidney, liver, lung, and spleen (5–7). When stimulated by agents associated with stress, NSMase2 is recruited into membrane domains typically referred to as lipid rafts (14, 15), by a mechanism thought to involve palmitoylation and hydrolyzes nonlysosomal SM to ceramide (Cer) (16, 17). It is well known that Cer and its metabolite sphingosine 1-phosphate (S1P) are interconvertible and both play important roles

* This work was supported, in whole or in part, by National Institutes of Health Grant NS36866-37 from the United States Public Health Service (to G. D.).
[S] This article contains supplemental Tables S1 and S2.
[1] To whom correspondence should be addressed: Dept. of Pediatrics MC4068, University of Chicago Pritzker School of Medicine, 5841 S. Maryland Ave., Chicago, IL 60637. Fax: 773-702-9234; E-mail: dawg@midway.uchicago.edu.

[2] The abbreviations used are: OI, osteogenesis imperfecta; Cer, ceramides; fro, fragilitas ossium; HA, hyaluronan; HAS2, hyaluronan synthase 2; HPTLC, high performance thin-layer chromatography; LC-MS/MS, liquid chromatography-tandem mass spectrometry; MβCD, methyl-β-cyclodextrin; NSMase2, neutral sphingomyelinase; PP2A, protein phosphatase 2A; S1P, sphingosine 1-phosphate; SM, sphingomyelin; mTOR, mammalian target of rapamycin; PTEN, phosphatase and tensin homolog deleted on chromosome 10.

in the regulation of cell proliferation, survival, and cell death (18–23). Cer usually inhibits cell proliferation and promotes apoptosis, whereas S1P stimulates growth and suppresses apoptosis (8).

Previous studies have reported that increased HA synthesis in skin fibroblasts can be correlated with severity of the disease in human OI patients (25–27) and hyaluronan synthetase (HAS) activities were higher in OI fibroblasts than in their controls. HA is a large, nonsulfated glycosaminoglycan composed of repeating D-glucuronic acid, (β1–3)*N*-acetyl-D-glucosamine (β1–4) units, which is found in body fluids and tissues, in both intra- and extracellular compartments. HA is crucial for cell proliferation, migration, and apoptosis, processes that control tissue remodeling during embryonic development, inflammation, injury, and cancer, and has long been associated with collagen mutations and malignant transformation of cells (28–30). HA is produced by three hyaluronan synthases (HAS1–3) in mammals. Knock-out mouse developmental studies show that HAS2 is essential but HAS1 and HAS3 have lesser roles (31, 32). HASs are membrane proteins containing multiple membrane domains and are likely lipid-dependent (particularly cardiolipin, CL) in Class I HASs (31, 33). It has been proposed that *Streptococcus equisimilis* HAS (SeHAS) contains an intraprotein core through which HA is synthesized and simultaneously translocated across the membrane to the cell exterior (34). Because methyl-β-cyclodextrin (MβCD) binds cholesterol, specifically down-regulates the expression of HAS2 and suppresses hyaluronan secretion in MCF-7 and smooth muscle cells (30, 35), it has been claimed that the maintenance of normal HA levels in cell cultures requires normal cell cholesterol homeostasis, and potentially intact cholesterol-rich microdomains termed lipid rafts (30, 35). Taking advantage of the *fro*/*fro* mouse model, we cultured fibroblasts from ear skin and observed a striking increase in HA synthesis, coupled with significant changes in cell morphology and cell cycle, which were consistent with that in skin fibroblasts from OI patients (25–27). This allowed us to further investigate the role of NSMase2, and its metabolite the bioactive sphingolipid Cer, in the mechanism of synthesis of HA. In this study, we found that increased expression of HAS2, through activation of the PI3K-PDK1-Akt-mTOR-p70S6K pathway, was dependent on regulation of the sphingolipid signaling molecule Cer and ceramide-associated protein phosphates 2A (PP2A). This is the first time a connection has been established between sphingolipid and glycosaminoglycan metabolism.

EXPERIMENTAL PROCEDURES

Standards and Reagents—Sph, DHSph, a 17-carbon analog of Sph (C_{17}-Sph), S1P, DHS1P, a 17-carbon analog of S1P (C_{17}-S1P), *N*-myristoyl (14:0), *N*-palmitoyl (16:0), *N*-oleoyl (18:1), *N*-stearoyl (18:0), *N*-arachidoyl (20:0), *N*-nervonoyl (24:1), *N*-lignoceroyl (24:0) sphingosines (ceramides (Cer)), *N*-palmitoyl (16:0), *N*-oleoyl (18:1), *N*-stearoyl (18:0), *N*-arachidoyl (20:0), *N*-behenoyl (22:0), *N*-nervonoyl (24:1), *N*-lignoceroyl (24:0), DHSph (dihydroceramides), *N*-heptadecanoyl sphingosine (17:0-Cer), and the palmitoyl (16:0), stearoyl (18:0), arachidoyl (20:0), behenoyl (22:0), nervonoyl (24:1), and lignoceroyl (24:0) coenzyme A substrates were obtained from Avanti Polar Lipids (Alabaster, AL). 3-Keto-DHSph was purchased from Matreya (Pleasant Gap, PA). The nonphosphorylated lipid standards were dissolved in methanol, whereas the sphingoid base phosphates were dissolved in methanol containing a trace amount of concentrated HCl and stored at −20 °C. [^{3}H]Palmitic acid (43 Ci/mmol) was purchased from PerkinElmer Life Sciences. Silica gel high performance thin-layer chromatography (HPTLC) plates were obtained from Whatman and the protein assay kit was obtained from Bio-Rad. Chloroform, methanol, and acetic acid used for HPTLC were of ACS grade and obtained from Fisher Scientific. VECTASHIELD mounting medium with 4′,6-diamidino-2-phenylindole (DAPI) was purchased from Vector Laboratories (Burlingame, CA). Hexamethylumbelliferyl phosphorylcholine was purchased from Moscerdam Substrates (Amsterdam, The Netherlands). C_2-ceramide and ceramides were from Sigma. S1P was purchased from Avanti Polar Lipids. RT-PCR primers for *Smpd3*, *Has1*, *Has2*, *Has3*, and 18S rRNA were obtained from Integrated DNA Technologies (Coralville, IA). The antibodies for NSMase2, HAS2, and p-Akt (Ser^{473}), p-Akt (Thr^{308}), and *p*-PP2A were obtained from Santa Cruz Biotechnology, HAS2, hyaluronan synthaseInc. (Santa Cruz, CA), and Akt, PI3K, *p*-PI3K, PDK1, *p*-PDK1, mTOR, *p*-mTOR, *p*-p70S6K, PTEN, and PP2A were from Cell Signaling Technology, Inc. (Danvers, MA), anti-Flotillin was from BD Transduction Laboratories (Franklin Lakes, NJ), β-actin antibody and secondary antibodies anti-mouse, anti-goat, and anti-rabbit were purchased from Sigma. Akt inhibitor VIII was from EMD Chemicals, Inc. (Gibbstown, NJ) and PI 3-kinase inhibitors LY294002 and wortmannin were purchased from Biomolecular Research Labs Inc. (Plymouth, Meeting, PA); NSMase inhibitor GW4869 and mTOR inhibitor rapamycin were purchased from Sigma. HA assay (K-1200) kits were from Echelon Biosciences (Salt Lake City, UT).

RT-PCR for NSMase2 and HAS1/2/3 mRNA Expression in Tissue and Cells—Total RNA was extracted from a variety of tissues and cultured fibroblasts by Qiagen RNeasy fibrous tissue mini kit and RNeasy mini kit (catalog numbers 74704 and 74104). RT-PCR was executed with a RT-PCR one-step kit (Qiagen, Valencia, CA) and primer pairs specific to mouse *Smpd3* (227 bp) using forward, 5′-ACATCGATTCTCCCACCAACACCT-3′, reverse, 5′-AATTCGCACAATGCAGCTGTCCTC-3′; primer pairs specific to mouse *Has1* (460 bp), using forward, 5′-GGAAAGCTTGACTCAGACACAAAGAC-3′ and reverse, 5′-AGGGAATTCGTATAGCCACTCTCGG-3′ primers; specific to mouse *Has2* (434 bp) using forward, 5′-ATGGATCCGCAAAAATGGGGTGGAA-3′ and reverse, 5′-GCGAATTCTAGTTGCATAGCCCAGA-3′ primers; specific to mouse *Has3* (237 bp) using forward, 5′-TAGGATCCCCAAGACTCGAAGCATC-3′ and reverse, 5′-CCGAATTCAACGGTAACGCAGGTGTCC-3′ primers; and 18S rRNA as control, using forward, 5′-CCAGAGCGAAAGCATTTGCCAAGA-3′ and reverse, 5′-AATCAACGCAAGCTTATGACCCGC-3′ primers. Briefly, the reaction mixture was prepared in PCR tubes according to the kit menu and put into a PerkinElmer GeneAMP PCR System 2400 (PerkinElmer Life Sciences). The programming RT-PCR procedure consisted of reverse transcription (50 °C for 30 min), initial PCR activation (95 °C for 15 min), then 35 cycles of 94 °C for 30 s, 55 °C for 30 s,

and 72 °C for 1 min, followed by a final extension at 72 °C for 10 min, annealing temperature may change according to primer T_m. The RT-PCR amplified samples were visualized on 1.2% agarose gels using ethidium bromide.

Generation of NSMase2$^{-/-}$ and ASMase$^{-/-}$ Mutant Mouse Fibroblast Cell Lines—Mouse skin fibroblasts were isolated from the ears of newly euthanized 2-week-old postnatal mice. Tissue fragments were plated in 20% bovine FCS in DMEM containing gentamycin and colonies of fibroblasts were trypsinized and subcultured. The Vector pCMV 3X-FLAG (Sigma) was used to transfect *Smpd3* and express NSMase2 in cultured skin fibroblasts. Stable clones were selected on the basis of neomycin (G418-sulfate) resistance.

Isolation of Detergent-resistant Membranes (Lipid Rafts)—Lipid rafts were isolated by their insolubility in Triton X-100 at 4 °C as described previously (13). Briefly, cell pellets were lysed in 1.5 ml of 25 mM MES, pH 6.5, 150 mM NaCl, 1.0% Triton X-100, 1 mM Na_3VO_4 supplemented with a protease inhibitor mixture (leupeptin, phenylmethylsulfonyl fluoride, and aprotinin) for 1 h at 4 °C. After homogenization 10 times in a loose-fit Dounce homogenizer, lysates were mixed with 1.5 ml of 80% sucrose in MBS (25 mM MES, pH 6.5, 150 mM NaCl) and overlayered with 3 ml of 30% sucrose in MBS and then with 3 ml of 5% sucrose in MBS. After centrifugation for 18 h at 31,000 × *g* in an SW40 rotor, 1-ml fractions were collected and analyzed. The raft fraction was typically found between fractions 3 and 4.

Western Blot Analysis—Lysates from fibroblast cell cultures and brain tissue were subjected to SDS-gel electrophoresis. Proteins were transferred to Immobilon-P membranes (Millipore, Bedford, MA), and Western blotting was carried out with antibodies according to the manufacturer's instructions. Positive bands were detected with a chemiluminescence kit from Fisher Scientific. The Western blot bands were scanned with a Bio-Rad ChemiDoc XRS and the images were quantified in Quantity One 4.5.0 software (Bio-Rad).

Immunostaining of Fibroblasts by Anti-HAS2—Fibroblasts were grown on 4-well tissue culture slides, rinsed twice in PBS, and fixed in cold 1:1 (v/v) methanol:acetone at −20 °C for 15 min, and then double-staining immunohistochemisty was executed. After removal of the fixative and rinsing three times with PBS, the slides were incubated in PBS, 1% Triton X-100 for 10 min at room temperature, then with PBS, 1% Triton X-100, 2% normal goat serum for 5 min at room temperature for a total of 15 min. The primary antibody anti-HAS2 was diluted in PBS, 1% Triton X-100, 2% normal goat serum and incubated with cells overnight at 4 °C. After rinsing six times with PBS for 5 min at room temperature, cells were incubated with FITC-conjugated secondary antibody (diluted in PBS, 1% Triton X-100, 2% normal goat serum) for 1 h, then rinsed in PBS at room temperature. 1 drop of VECTASHIELD mounting medium with 4′,6-diamidino-2-phenylindole (DAPI) was added to each well and the slide sealed with nail polish. The immunofluorescence reaction was followed and documented with an Axiovert S100 TV (Carl Zeiss, Inc.).

Sphingomyelinase Assay—NSMase activity was determined with the fluorogenic substrate hexamethylumbelliferyl phosphorylcholine as described previously (11), and also by the Echelon Sphingomyelinase Kit (K-1800) as described in the manufacturer's protocol. Briefly, cells were harvested and washed with PBS, the pellets were resuspended and lysed in 25 mM Tris-HCl, 150 mM NaCl, and 1% Triton X-100, pH 7.4, 50 mg of protein were mixed with the fluorogenic substrate hexamethylumbelliferyl phosphorylcholine. The incubation was carried out at pH 7.4 in 100 mM Tris-HCl buffer containing 10 mM $MgCl_2$ and 5 mM DTT to block any ASMase activity. The hexamethylumbelliferyl released was followed fluorometrically in a 96-well FLX microplate reader. The enzyme activity was calculated from the slope of the graph of intrinsic fluorescence plotted against time and standardized by milligrams of protein.

Analysis of Lipid Synthesis by HPTLC—Cells were labeled with [^{3}H]palmitate and lipids were extracted as described previously (36). Typical labeling experiments were carried out in 100-mm Petri dishes containing 8 ml of serum-free medium for 24 h. Cells (3×10^6/100-mm plate) were harvested and washed three times with phosphate-buffered saline, lipids were extracted by chloroform:methanol:water (2:1:0.6, v/v) partition and samples were subjected to alkaline methanolysis to remove phosphoglycerides. Lipids were applied to HPTLC plates (10 × 10 cm; LHP-K TLC plates, Whatman, Inc.) and developed in chloroform:methanol:glacial acetic acid:water (70:25:8.8:4.5, v/v). Lipids were visualized in iodine vapors, then scraped off for quantification. Mouse brain (0.1 g) lipids were extracted by 1.2 ml of H_2O, 2 ml of methanol, and 4 ml of chloroform, and then subjected to alkaline methanolysis to remove phosphoglycerides. Lipids were applied to HPTLC plates and developed in chloroform:methanol:glacial acetic acid:water (70:25:8.8:4.5, v/v), sphingomyelin was visualized by charring with 10% $CuSO_4$, 8% H_2SO_4.

Lipid Extraction and Sample Preparation for Lipid Quantification by LC/MS/MS—Cellular lipids were extracted by a modified Bligh and Dyer (37) procedure with the use of 0.1 N HCl for phase separation. C_{17}-S1P (40 pmol), C_{17}-Sph (30 pmol), and 17:0-Cer (30 pmol) were used as internal standards and were added during the initial step of lipid extraction. The extracted lipids were dissolved in methanol:chloroform (4:1, v/v), and aliquots were taken to determine the total phospholipid content as described previously (38). Samples were concentrated under a stream of nitrogen, redissolved in methanol, transferred to autosampler vials, and subjected to consecutive LC/MS/MS analysis of sphingoid bases, ceramides, and sphingoid base 1-phosphates.

Analysis of Sphingoid Bases, Sphingoid Base 1-Phosphates, and Ceramides—Analyses of sphingolipids were performed by combined LC/MS/MS using an automated Agilent 1100 series liquid chromatograph and autosampler (Agilent Technologies, Wilmington, DE) coupled to an API4000 Q-trap hybrid triple quadrupole linear ion trap mass spectrometer (Applied Biosystems) equipped with a TurboIonSpray ionization source. Sphingolipids were ionized via electrospray ionization with detection via multiple reactions monitoring. Analysis of sphingoid bases and the molecular species of ceramides used electrospray ionization in positive ions with multiple reactions monitoring analysis (39). Standard curves for each of the sphingoid bases, sphingoid base 1-phosphates, and ceramides molecular species were constructed by adding increasing concentrations of the individual analyte to 30 or 40 pmol of the corresponding struc-

tural analogs used as the internal standard. Linearity and the correlation coefficients of the standard curves were obtained by a linear regression analysis. The standard curves were linear over the range of 0.0–300 pmol of each of the sphingolipid analytes with correlation coefficients (R^2) > 0.98.

Hyaluronan Production Assay—Fibroblasts were seeded in DMEM, 10% FBS, 1% gentamycin at 10^6/100-mm dish. Cell culture conditioned media were collected after 7 days for hyaluronan quantification, whereas cells were quantified for protein. In inhibitors and sphingolipid (ceramide and S1P) treatment experiments, Akt inhibitor VIII (5 μM), PI 3-kinase inhibitors LY294002 (25 μM) and wortmannin (5 μM), mTOR inhibitor rapamycin (5 nM), NSMase2 inhibitor GW4869 (1 μM), C_2-ceramide (5 and 10 μM), and ceramides (5 μM) were added to the cell culture, conditioned media were collected after 72 h treatment. The HA level was determined with the competitive ELISA kit from Echelon Biosciences according to the manufacturer's instructions. Briefly, samples of conditioned media were first mixed with the detector (the HA-binding protein), then added to the HA ELISA plate for competitive binding. The colorimetric signal (hydrolyzed *p*-nitrophenyl phosphate) was detected at 405 nm with a PerkinElmer VICTOR^{3}® 1420 Multilabel Counter and inversely correlated with the amount of HA present in the samples.

Gene Expression Profiling—RNA was extracted from fibroblasts with TRIzol and Qiagen kits, and RNA integrity was assessed with an Agilent 2100 Bioanalyzer. High-quality RNA (RNA integrity number >9.0) was used for expression microarray analysis in which 2 μg of the total RNA was processed for biotin-labeled target preparation and hybridization to the Affymetrix mouse genome 430 2.0 Genechip expression arrays according to the Genechip Expression analysis technical manual (Affymetrix, Inc.). After hybridization for 16 h at 45 °C with rotating at 60 rpm, arrays were washed and stained on a GeneChip Fluidics Station (Affymetrix, Inc.) and scanned using the Gene Chip Scanner 3000 7G. The CEL intensity data extracted by GCOS (Gene Chip Operating Software) were used for data analysis. Functional analysis of statistically significant gene expression changes were performed with Ingenuity Pathways Analysis (IPA, Ingenuity Systems) and DNA-Chip Analyzer (dChip) software. Ingenuity Pathways Analysis software analyses RNA expression data in the context of known biological response and regulatory networks as well as other higher-order response pathways. Ingenuity functional analysis identified biological functions and/or diseases that were most significant. Only genes from the data set that met the 2-fold ($p < 0.01$) change cutoff and were associated with biological functions in the Ingenuity Pathways Knowledge Base were considered for further analysis. dChip is a Windows software package for probe-level (*e.g.* Affymetrix platform) and high-level analysis of gene expression microarrays, at the probe level. dChip can display and normalize the CEL files, and the model-based approach allows pooling information across multiple arrays. The gene information and sample information were correlated with the analytical results.

Statistical Analysis—The results of LC-MS/MS analyses are from duplicate experiments run in triplicate. The cell death assay results are from duplicate experiments run in triplicate. Statistical analyses were performed by Student's *t* test, and results were considered statistically significant when $p < 0.05$.

RESULTS

The Importance of Nonlysosomal NSMase2 in Regulating Ceramide Levels—RT-PCR analysis showed that although the highest level of expression of the gene for NSMase2 (*Smpd3*) is in brain and bone, there is significant expression in skin but very little in the heart, kidney, liver, and spleen (Fig. 1*A*). Therefore we used fibroblasts from the *fro*/*fro* mouse to discover the function of NSMase2. At the same time we also cultured fibroblasts from the Niemann-Pick (*Smpd1*$^{-/-}$) mouse (deficient in lysosomal ASMase) for comparison. Western blot analysis showed only a 70-kDa NSMase2 band in ossium fragilis (*fro*/*fro*) mouse brain compared with the major 72-kDa and minor 70-kDa bands in heterozygotes (Fig. 1*B*). Enzyme analysis showed NSMase2 activity to be absent from *fro*/*fro* fibroblasts compared with its wild type (Fig. 1*C*). Labeling of cells with [^{3}H]palmitate showed accumulation of SM and cholesterol in *fro*/*fro* fibroblasts (Fig. 1*D*), and the lipid changes were mostly corrected by transfection with *Smpd3*. LC/MS/MS analysis showed that ceramide levels were lower by 50% in *fro*/*fro* mouse fibroblasts, calvaria (bone), and brain (Fig. 1*E*), but were minimally affected in ASMase$^{-/-}$ fibroblasts and unaffected in ASMase$^{-/-}$ brain (data not shown); in contrast SM is greatly elevated in ASMase$^{-/-}$ tissues. In addition, LC/MS/MS analysis also revealed that in the *fro*/*fro* (NSMase2$^{-/-}$) fibroblasts, the reduction in ceramides was across the board in terms of fatty acid content and absolute levels. C16:0-, C24:0-, and C24:1-ceramide molecular species were the major ceramides in fibroblasts compared with C18:0-ceramide in the brain (40) (Fig. 1*F*). Thus the fibroblast brain differences may be explained by differential expression of ceramide synthases (41).

Analysis of fro/fro and ASMase$^{-/-}$ *Fibroblasts*—The *fro*/*fro* mice showed slow growth and severe skeletal deformities, including frequent bone fractures, unlike the ASMase$^{-/-}$ mice, which showed symptoms of a neurovisceral lysosomal storage disease (42, 43). Cultured fibroblasts from *fro*/*fro* mice demonstrated slow growth and aberrant morphology compared with normal control but this could be reversed by transfection with *Smpd3.* Microarray gene expression analysis (dChip) of cultured *fro*/*fro* fibroblasts, compared with wild type cells, showed 3 significantly altered pathways out of 83 analyzed (namely, cell cycle, DNA replication and G_1 to S cell cycle), the expression of growth related genes such as cyclins (Ccna2, Ccnb1, Ccnb2, Ccnb11, Ccne1, and Ccne2) was down-regulated, whereas expression of p15 and p21 (cyclin-dependent kinase inhibitors 1A and 2B) was up-regulated (supplemental Table S1, *a*–*d*). Cell growth abnormalities of the *fro*/*fro* (NSMase2$^{-/-}$) fibroblasts were confirmed by flow cytometric analysis of the cell cycle, whereas ASMase$^{-/-}$ fibroblasts grew normally (data not shown). Biofunctional analysis identified tissue, skeletal and muscular system development, and functional changes (supplemental Table S2), suggesting that study of *fro*/*fro* fibroblasts could provide insights into the sphingolipid regulation of connective tissue and growth.

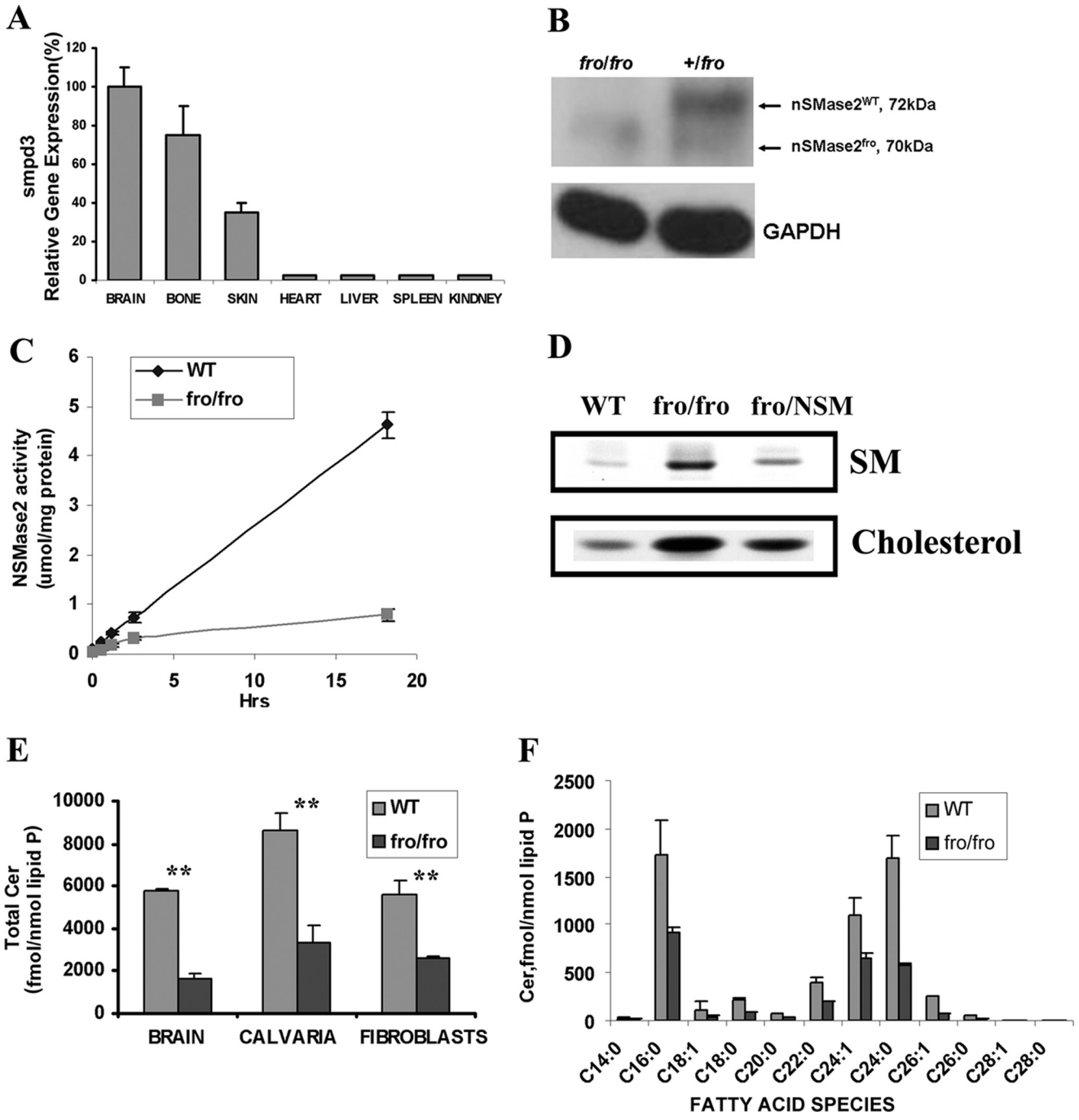

FIGURE 1. **Differential expression of NSMase2 in mouse tissues and the effect of deletion of NSMase2 activity on sphingolipids in *fro*/*fro* mouse brain, bone, calvaria, and skin fibroblasts.** *A*, RT-PCR showed that the expression of *Smpd3* in mouse tissues was highest in brain and bone, with lesser expression in skin, and very little in heart, kidney, liver, and spleen. *B*, Western blot analysis of brain lysates from 3-month-old littermates exposed to anti-NSMase2 antibody (sc-67305) at 1:500 dilution showed the expression of a 70-kDa truncated protein in *fro*/*fro* compared with the major 72-kDa band in the (+/*fro*) heterozygote (*right-hand lane*). *C*, NSMase2 activity (assayed as described in the text) showed NSMase2 activity to be depleted in *fro*/*fro* fibroblasts. *D*, storage of sphingomyelin and cholesterol was observed in *fro*/*fro* (NSMase2$^{-/-}$) fibroblasts as described in the text. Transfection with the *Smpd3* gene (*fro*/*NSM*) reversed the increase in SM. *E*, LC/MS/MS analysis as described in the text revealed a >50% reduction of ceramides in *fro*/*fro* (NSMase2$^{-/-}$) brain, calvaria, and fibroblasts compared with wild type. *F*, LC-MS/MS analysis showed all ceramide fatty acid species to be decreased in NSMase2$^{-/-}$ fibroblasts compared with wild type. Results are representative of three independent experiments.

Increased Hyaluronan Synthesis and HAS2 Expression in fro/fro Fibroblasts—The elevated HA in *fro*/*fro* fibroblasts compared with WT was confirmed by direct HA analysis (Fig. 2*A*). The increased expression of hyaluronan synthase-2 was shown by RT-PCR, Western blot, and immunocytochemistry (Fig. 2, *B–D*). HA levels in *fro*/*fro* were 15-fold higher than in controls (Fig. 2*A*). RT-PCR showed that expression of *Has2* was increased 6-fold (Fig. 2*B*) but that *Has1* levels were unchanged. *Has3* was not detected in mouse skin fibroblasts. The Affymatrix gene analysis also supported these unexpected findings. Transfection of *Smpd3* decreased both the expression of HAS2 and the production of HA (Fig. 2, *E*

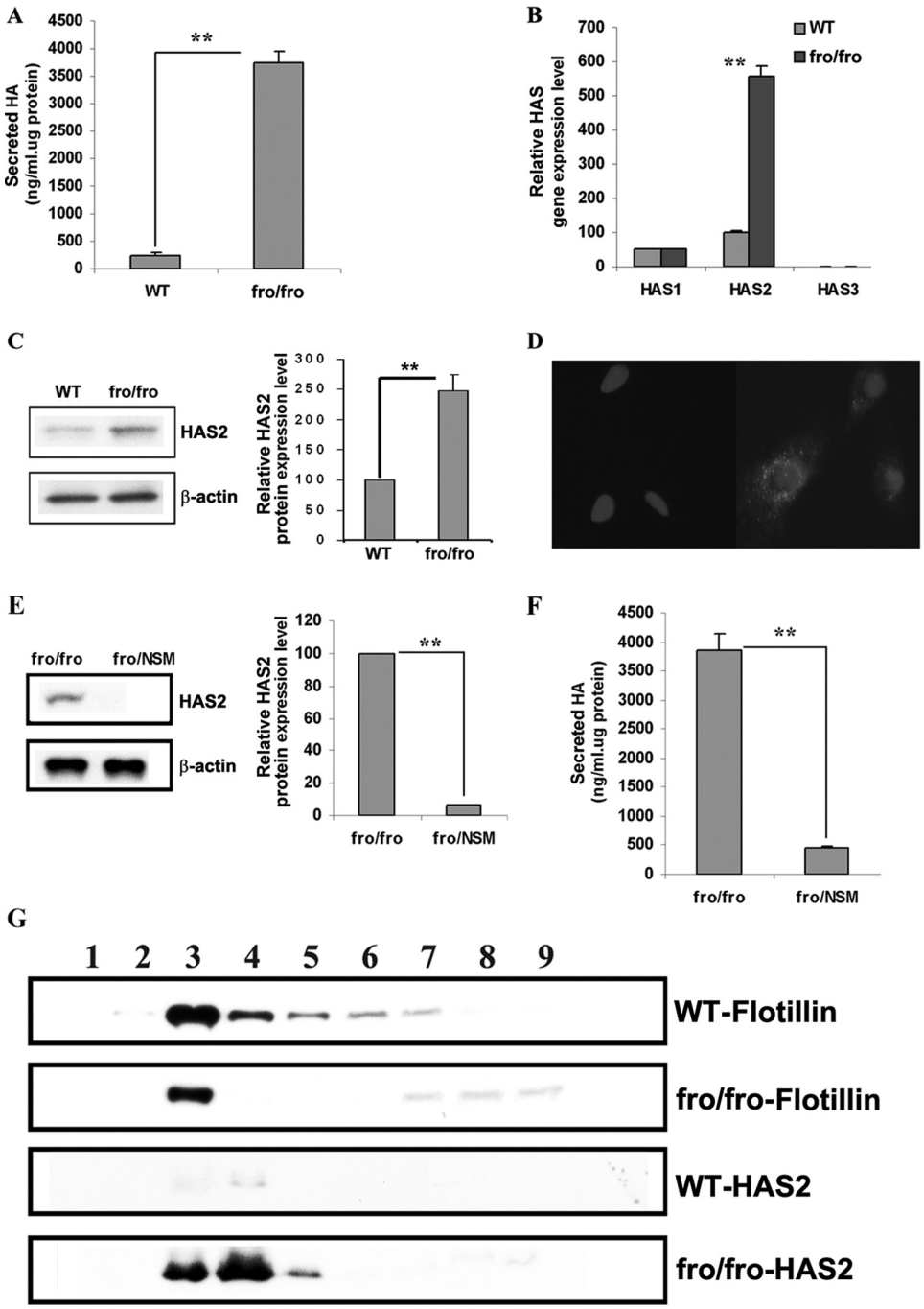

FIGURE 2. **Increased expression of HAS2 is associated with increased production of HA in *fro/fro* (NSMase2$^{-/-}$) fibroblasts.** *A*, the amount of hyaluronan (*HA*) in 7-day conditional culture medium from *fro/fro* (NSMase2$^{-/-}$) fibroblasts was >15-fold higher than that in WT culture media. HA levels were determined with a competitive ELISA kit from Echelon Biosciences (catalog number K-1200) according to the manufacturer's instructions. *B*, RT-PCR showed significantly increased expression of *Has2* but not *Has1* and *Has3* in *fro/fro* (NSMase2$^{-/-}$) fibroblasts. *C*, Western blot showed increased HAS2 protein in *fro/fro* (NSMase2$^{-/-}$) fibroblasts compared with WT. *Left panel*, Western blot; *right panel*, quantification corrected for protein. *D*, increased HAS2 immunostaining of *fro/fro* (NSMase2$^{-/-}$) fibroblasts compared with WT. *E*, transfection of the *fro/fro* (NSMase2$^{-/-}$) fibroblasts with *Smpd3* reversed the increased HAS2 expression. *Left panel*, Western blot; *right panel*, quantification corrected for protein. *F*, transfection of the *fro/fro* (NSMase2$^{-/-}$) fibroblasts with *Smpd3* also reversed the increased HA synthesis. *G*, increased HAS2 expression is associated with lipid rafts in the *fro/fro* (NSMase2$^{-/-}$) fibroblasts. Western blot analysis using anti-flotillin and anti-HAS2 antibodies (as described in the text) showed the association of HAS2 and flotillin (lipid rafts fractions 3/4 marker), and increased lipid rafts HAS2 in the *fro/fro* (NSMase2$^{-/-}$) fibroblasts compared with WT. The procedures are as described in the text and results are representative of three independent experiments.

and *F*) in *fro/fro* fibroblasts. Because HAS1/2/3 are membrane proteins, Kullti *et al.* (30) used raft-disrupting detergent methyl-β-cyclodextrin to show that intact membrane microdomains were critical for HAS2 activity. By using lipid raft isolation we were able to verify that there was more HAS2 expressed in the lipid rafts microdomain (flotillin-positive fractions 3 and 4) in *fro/fro* fibroblasts than in WT (Fig. 2*G*). In contrast, the secretion of HA was decreased in lysosomal ASMase$^{-/-}$ fibroblast culture medium compared with its control (the amounts of HA in both were low),

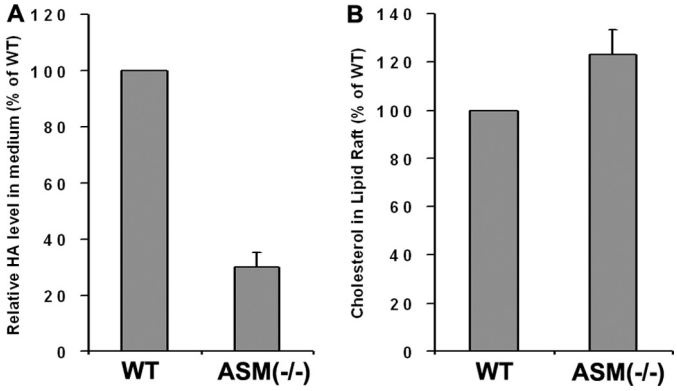

FIGURE 3. **Decreased production of HA in ASMase$^{-/-}$ fibroblasts is associated with elevated storage of cholesterol in lipid rafts.** *A*, decreased production of HA in ASMase$^{-/-}$ fibroblast culture medium. *B*, increased cholesterol in lipid rafts from ASMase$^{-/-}$ fibroblasts. The procedures are as described in the text and results are representative of three independent experiments.

although the cholesterol levels were elevated in isolated ASMase$^{-/-}$ fibroblast lipid rafts (Fig. 3, *A* and *B*).

Activation of Akt Signaling Pathway in fro/fro (NSMase2$^{-/-}$) Fibroblasts—We detected increased p-Akt in *fro*/*fro* fibroblasts, and surprisingly found a higher constitutive expression of Akt in *fro*/*fro* fibroblasts compared with a lower expression of Akt in ASMase$^{-/-}$ fibroblasts and controls (Fig. 4, *A* and *B*). Consistently, Akt phosphorylation at both threonine 308 (Akt-Thr^{308}) and serine 473 (Akt-Ser^{473}) was elevated in *fro*/*fro* mouse skin fibroblasts, but decreased in ASMase$^{-/-}$ fibroblasts (Fig. 4, *A* and *B*). Higher constitutive expression and phosphorylation of Akt in *fro*/*fro* fibroblasts could be reversed by transfection with *Smpd3* (Fig. 4, *A* and *B*). Phosphorylation of Akt on Thr^{308} in its activation loop is necessary and sufficient for Akt activation although the activation and regulation may be dependent on a dual regulatory mechanism that requires both its translocation to the plasma membrane, and dual phosphorylation on Thr^{308} and Ser^{473} by PDK1 and the TORC2 complex. We then showed that activation of PDK1 (which activates Akt at Thr^{308}) occurred only in *fro*/*fro* fibroblasts (Fig. 4, *C* and *D*) and not in ASMase$^{-/-}$ fibroblasts. Finally, we showed activation of signaling molecules downstream of Akt, namely mTOR and p70S6K (Fig. 4, *C* and *D*). Because PTEN can regulate the activity of Akt by hydrolyzing its lipid activator Phosphatidylinositol (3,4,5)-trisphosphate (PIP_3) we determined the level of PTEN and found no change (Fig. 4*E*). Although there was no change in PP2A by Western blot analysis we did observe a decrease in *p*-PP2A and this was a critical connection with decreased ceramides because ceramide activates PP2A (Fig. 4*F*) (44). The microarray data also showed a 6-fold increased expression of PI3K, which is an upstream signaling molecule in the Akt cascade (Fig. 5*A*), and this was confirmed by Western blot analysis showing increased expression and phosphorylation of PI3K (Fig. 5, *B*–*D*).

Correlation of Production of HA with NSMase2 and Signaling Molecules of PI3K-Akt-mTOR Pathway in Fibroblasts—We hypothesized that inhibitors of the PI3K-Akt-mTOR pathway should inhibit HA synthesis. By adding inhibitors, we were then able to show that treatment of *fro*/*fro* fibroblasts with Akt inhibitor VIII inhibited elevated expression and phosphorylation of Akt (Fig. 6, *A* and *B*), and that both Akt inhibitor VIII (5 μM) and PI 3-kinase inhibitors LY294002 (25 μM) and wortmannin (5 μM) were able to reduce HA secretion (Fig. 6*C*). The nonspecific inhibitor of mTOR (rapamycin) (5 nM) also partly reduced the production of HA in *fro*/*fro* fibroblasts culture (Fig. 6*D*). In contrast, the specific NSMase2 inhibitor GW4869 (1 μM) increased the secretion of HA (Fig. 6*E*).

Regulation of Expression of Akt and Production of HA by Bioactive Sphingolipids Ceramide and S1P—We previously showed that C_2-ceramide could decrease Akt phosphorylation in F11 cells (most likely through activation of a phosphatase) (45), whereas S1P has the opposite effect in human glioblastoma cells (46–48). This was confirmed in mouse fibroblasts. Treatment of fibroblasts with 20 μM C_2-ceramide or 400 nM S1P had the opposite effect on Akt phosphorylation in that C_2-ceramide inhibited and S1P stimulated (Fig. 7, *A* and *B*). Because Cer and S1P are interconvertible, we investigated the changes in the level of S1P when Cer was reduced in *fro*/*fro* fibroblasts. Through analysis by LC/MS/MS we found that although the Cer/S1P ratio was decreased, the absolute amount of S1P was also decreased (Fig. 7*C*). Because the phosphorylation of PP2A was decreased in *fro*/*fro* fibroblasts (because of reduced Cer), the increased expression and phosphorylation of Akt was most likely the result of decreased Cer. This was confirmed by showing that exogenous C_2-ceramide (5 and 10 μM) and mixed ceramides (5 μM) decreased the production of HA in *fro*/*fro* fibroblasts (Fig. 7*D*). Based on our results, the most likely mechanism is that reduced nonlysosomal Cer levels cause inactivation of PP2A (44) and activation of the PI3K-Akt-mTOR pathway leading to increased *Has2* gene transcription in *fro*/*fro* fibroblasts.

DISCUSSION

Previous studies showed that multiple cell behaviors including cell proliferation, migration, and apoptosis are influenced by the glycosaminoglycan composition of the extracellular matrix with a major role for HA (29, 49–52). The fibroblasts cultured from a OI patient produced increased HA (25–27), and in this study the elevated HA has also been found in cultured fibroblasts from *fro*/*fro* mice, an animal model of OI. Because *fro*/*fro* is from a spontaneous deletion in the *Smpd3* gene (encoding NSMase2, an important enzyme in sphingolipid metabolic pathway), this suggested the possibility that sphingolipids may regulate the synthesis of HA.

HA is synthesized by three membrane hyaluronan synthases (HAS1/2/3) (31) but we find only HAS2 is increased over normal levels in *fro/fro* (NSMase2$^{-/-}$) fibroblasts and is predominantly in plasma membrane microdomains called "lipid rafts" (14, 15). This is consistent with a model proposed by Kultti *et al.* (30), in which the disruption of lipid rafts by the exogenous detergent MβCD interfered with a chain of events from PI3K to Akt/mTOR, leading to decreased synthesis of HA through inhibition of HAS2 in MCF-7 cells. They concluded that intact membrane microdomains were critical for HAS2 activity and that enrichment of cholesterol/SM promotes microdomains, which are thicker, more lipid-ordered and therefore more stable (30). They also observed decreased phosphorylation of Akt (specifically at Thr^{308}) and its downstream target p70S6K when

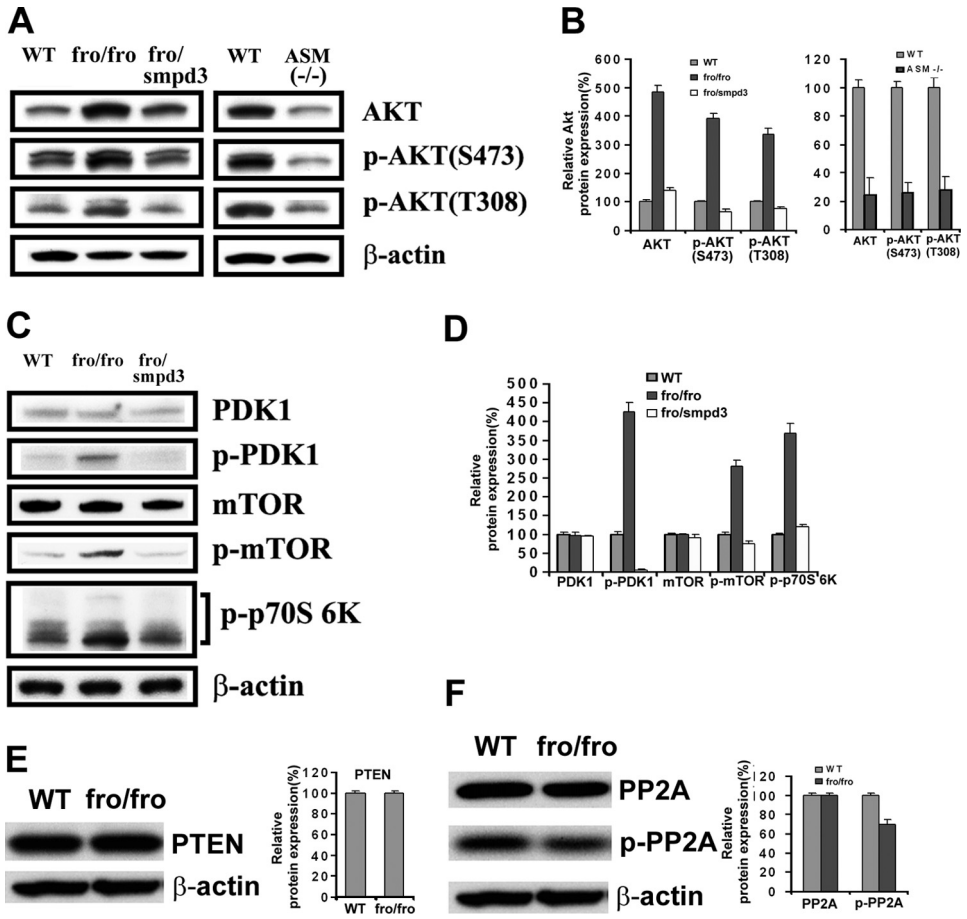

FIGURE 4. **Increased expression and phosphorylation of Akt and related signaling molecules in *fro/fro* fibroblasts.** *A*, Western blot showed increased expression and phosphorylation of Akt in *fro/fro* (NSMase2$^{-/-}$) fibroblasts (*second lane 2*) compared with WT (*first lane*) and the reversal following transfection with *Smpd3* (*third lane*). In contrast, the expression and phosphorylation of Akt was decreased in ASM$^{-/-}$ fibroblasts (*fifth lane*) compared with WT (*fourth lane*). *C*, Western blot showed increased phosphorylation of PDK1, mTOR, and p70S6K in *fro/fro* (NSMase2$^{-/-}$) fibroblasts (*second lane*) compared with WT (*first lane*) and reduction in *p*-PDK1, *p*-mTOR, and *p*-p70S6K after *Smpd3* transfection of fibroblasts (*third lane*). *B* and *D* show quantification corrected for protein. *E*, Western blot showed unchanged expression of PTEN (*left panel*) in *fro/fro* (NSMase2$^{-/-}$) fibroblasts (*second lane*) compared with WT (*first lane*) with the quantification corrected for the protein (*right panel*). *F*, Western blot showed decreased phosphorylation of PP2A (*left panel*) in *fro/fro* (NSMase2$^{-/-}$) fibroblasts (*second lane*) compared with WT (*first lane*) and quantification corrected for protein (*right panel*). Treatment details are given in the text and results are representative of three independent experiments.

HAS2 was suppressed. A similar study by Sakr *et al.* (35) in cultured aortic smooth muscle cells from Watanabe heritable hyperlipidemic rabbits and New Zealand White rabbits suggested that normal HA levels in cell cultures required normal cell cholesterol homeostasis (35). Although both studies discussed the importance of cholesterol (lipid rafts) in maintaining HA levels and HAS2 activity, there was no deep discussion about the active regulation of expression of the gene. By adding exogenous cholesterol and MβCD to cells, Sakr *et al.* (35) tried to explain that elevated accumulation of HA depended on cellular or membrane cholesterol content, although the effect of exogenous cholesterol to HA in Watanabe heritable hyperlipidemic aortic smooth muscle cells was minor. Analysis of ASMase$^{-/-}$ fibroblasts showed that cholesterol levels were elevated in lipid rafts but secreted HA was decreased compared with normal. SM is accumulated in both *fro/fro* and ASMase$^{-/-}$ fibroblasts, but previous studies have also shown that SM accumulation is not restricted to lysosomes when ASMase is lacking. Thus the lysosomal membranes contained 6.1-fold more SM than the WT but nonlysosomal membranes also showed a significant 4.8-fold SM increase in the ASMase$^{-/-}$ mouse (53). Therefore increased SM in lipid rafts seems unlikely to be the factor that regulates expression of the *Has2* gene. In our study, we found that NSMase2 generated Cer was the most critical factor in regulating HA synthesis in *fro/fro* fibroblasts.

NSMase2 is palmitoylated, has two transmembrane regions and an optimal activity at pH 7.4, whereas ASMase is soluble, undergoes complex post-translation processing typical of many lysosomal hydrolases (17, 54) and has an acid pH optimum at pH 4.5. Thus they are active in plasma membrane and lysosomal compartments, respectively (55). In *fro/fro* (NSMase2$^{-/-}$) fibroblasts both SM and cholesterol accumulate, and ceramide decreases. This is consistent with the hypothesis of Sakr and Kultti (30, 35) that the enhanced ordered plasma membrane structure (lipid rafts) is conductive to stable activity of HAS2 and HA synthesis. We observed that HA was overproduced because of activation of HAS2 and by Western blot we were able to actually demonstrate the increased presence of HAS2 in lipid rafts. The transfection of *Smpd3* into *fro/fro* fibroblasts decreased HAS2 expression and HA accumulation. In contrast, addition of the NSMase2-specific inhibitor

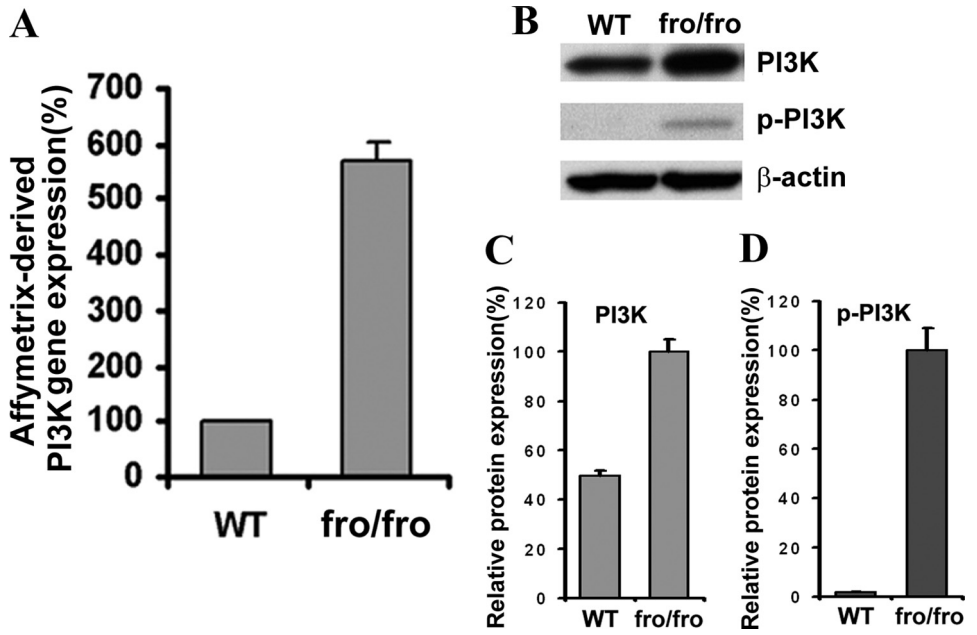

FIGURE 5. **Loss of NSMase2 activity increases PI3K expression.** *A*, microarray data showed increased PI3K expression in *fro/fro* (NSMase2$^{-/-}$) fibroblasts compared with WT. *B*, Western blot confirmed increased expression and phosphorylation of PI3K in *fro/fro* (NSMase2$^{-/-}$) fibroblasts (*second lane*) compared with WT (*first lane*). *C* and *D* show quantification corrected for protein. Results are representative of three independent experiments.

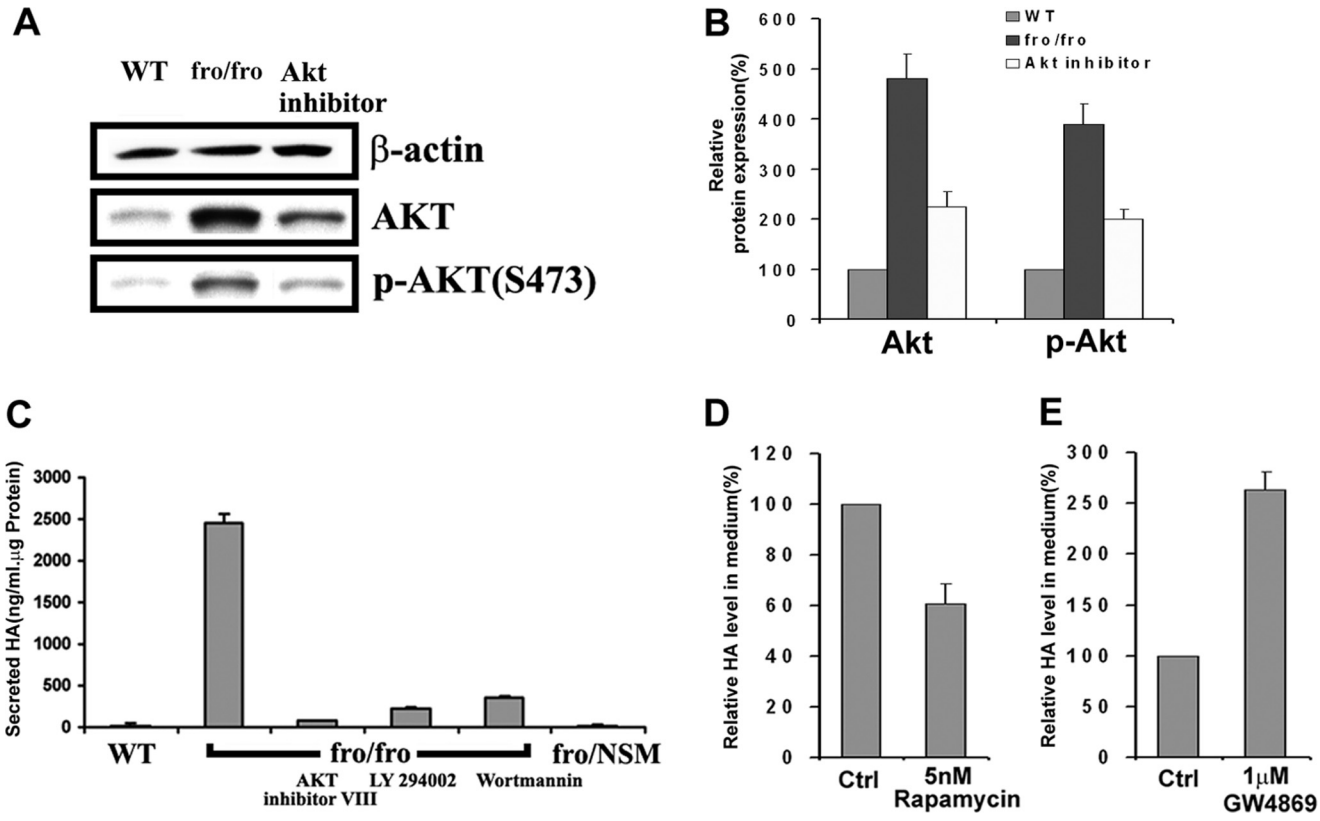

FIGURE 6. **HA synthesis is associated with increased expression and activation of Akt and related signaling molecules.** *A*, Western blot of WT (*first lane*), *fro/fro* (NSMase2$^{-/-}$) (*second lane*), and in the presence of Akt inhibitor VIII (*third lane*) showed reversal of the increase of the expression and phosphorylation of Akt. *B*, *bar graphs* show quantification corrected for protein for Akt and phosphorylated Akt (*p-Akt*). *C*, correlation of decreased HA synthesis and decreased expression and phosphorylation of Akt (*A*) by showing >90% decreased production of HA in the presence of Akt VIII inhibitor, and PI3K inhibitor LY294002 or wortmannin in *fro/fro* (NSMase2$^{-/-}$) fibroblasts. *D*, mTOR inhibitor rapamycin (5 nM) reduced the production of HA in fibroblasts by 40%, implicating mTOR involving the production of HA. *E*, production of HA was increased 2.5-fold by adding 1 μM NSMase2 inhibitor GW4869 to fibroblasts. The procedures are as described in the text and results are representative of three independent experiments.

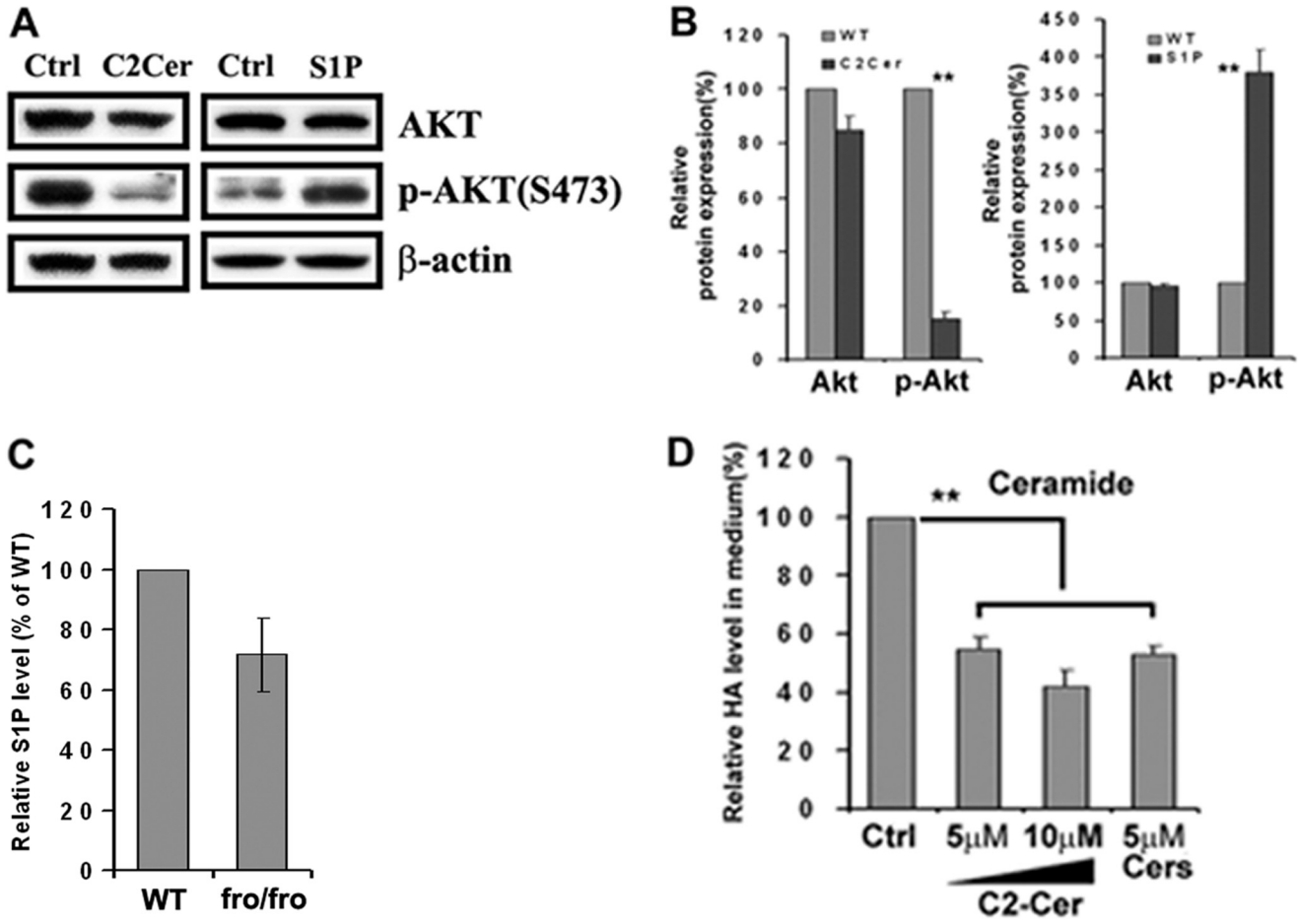

FIGURE 7. **Sphingolipids (ceramides and S1P) regulate the expression and phosphorylation of Akt and production of HA.** *A*, Western blot showed decreased phosphorylation of Akt in fibroblasts after treatment with 20 μM C_2-ceramide (*second lane*) compared with its control (*first lane*). The Western blot also showed increased phosphorylation of Akt in fibroblasts after treatment with 400 nM sphingosine 1-phosphate (S1P) (*fourth lane*) compared with its control (*third lane*). *B*, *bar graphs* showed the relative changes in protein expression of Akt and phosphorylation of Akt. *C*, S1P is decreased in *fro*/*fro* fibroblasts compared with WT. *D*, exogenous C_2-ceramide (5 and 10 μM) and 5 μM mixed ceramides reduced the production of HA in fibroblasts by 50%. Analyses were carried out by LC-MS/MS as described in the text. Other procedures are as described in the text and results are representative of three independent experiments.

GW4869 to control fibroblasts produced more HA, indicating that NSMase2 was correlated to the synthesis of HA. Compared to *fro*/*fro* fibroblasts, the synthesis of HA was decreased in ASMase$^{-/-}$ fibroblasts, although cholesterol accumulated in its lipid rafts. Kultti *et al.* (30) observed decreased phosphorylation of Akt specifically at Thr^{308} by adding MβCD to MCF-7 cells. We found increased expression of Akt and phosphorylation in both Thr^{308} and Ser^{473} sites in *fro*/*fro* fibroblasts, but decreased expression and phosphorylation in both Thr^{308} and Ser^{473} sites in ASMase$^{-/-}$ fibroblasts. Addition of Akt inhibitor VIII to *fro*/*fro* fibroblasts inhibited the expression and phosphorylation of Akt and HA accumulation was reduced, suggesting that Akt was involved in HA production. Besides Akt, the other signaling molecules in the PI3K-PDK1-Akt-mTOR-p70S6K pathway were also up-regulated, but no abnormalities occurred in PTEN expression. Previous studies showed that activation of the PI3K/Akt/mTOR pathway was often accompanied by the loss of PTEN (56), and we also have previously shown PTEN to be active in lipid rafts (57). By addition of PI3K, Akt, and mTOR inhibitors, we could reduce HA accumulation. The increased *Has2* gene expression most likely involves NFκB, because it has functional binding sites in the HAS2 promoter (58). The transfection of *Smpd3* reversed increased expression and phosphorylation of Akt in *fro*/*fro* fibroblasts. Because increases in ceramide have been shown to reduce the level of p-Akt in MCF-7 cells either by inactivating the Akt kinase or activating the PP2A phosphorylase by dephosphorylating p-Akt (45, 48), it is important to demonstrate here that the reduction in ceramide levels by NSMase2$^{-/-}$ could cause the activation of Akt in *fro*/*fro* fibroblasts, together with a decrease in *p*-PP2A (active PP2A). The regulation of Akt by Cer was verified by adding C_2-Cer to fibroblasts, and exogenous Cer also reduced the amount of HA synthesized. In contrast, both the expression and phosphorylation of Akt and HA secretions were decreased in ASMase$^{-/-}$ fibroblasts by an unknown mechanism. It has been proposed that Class I HASs are lipid-dependent (31, 33) and that specific phospholipids are required for activity of membrane-bound SeHAS and *Mus musculus* HAS2 (31, 33). At the present time we cannot rule out a role for S1P because the balance of Cer/S1P (the "rheostat" theory) (59) was decreased in *fro*/*fro* mice compared with ASMase$^{-/-}$ mice.

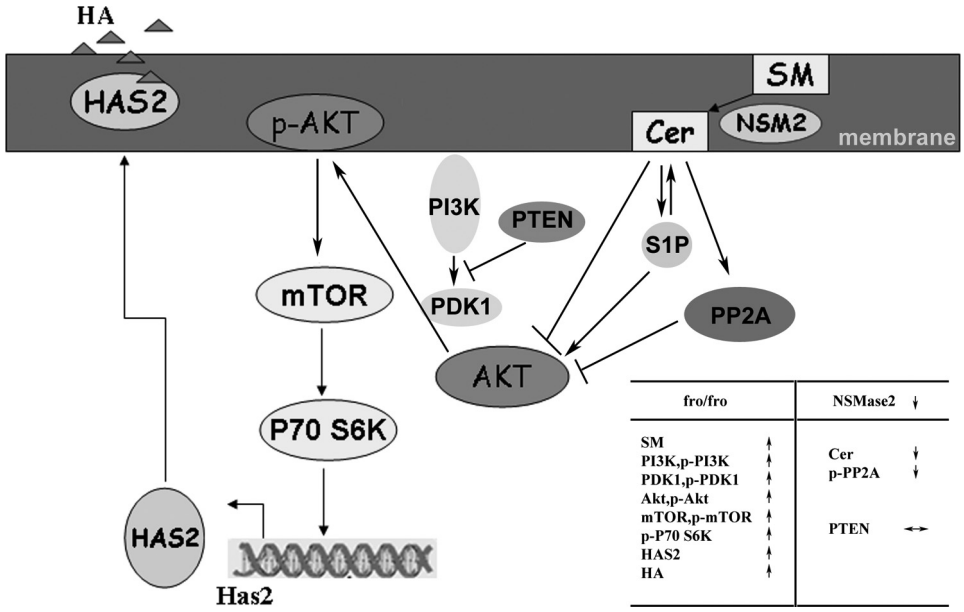

FIGURE 8. **A scheme to explain the increased production of HA in *fro*/*fro* (NSMase2$^{-/-}$) mouse fibroblasts.** The NSMase2 gene deletion reduces Cer by 50% in *fro*/*fro* fibroblasts, the decreased Cer induces decreased phosphorylation and activity of PP2A, increased expression and phosphorylation of PI3K, PDK1, AKT, mTOR, and p70S6K leading to increased expression of HAS2 and synthesis of HA. Transfection of the *Smpd3* gene into *fro*/*fro* (NSMase2$^{-/-}$) fibroblasts or addition of exogenous C_2-ceramide reverses the increased phosphorylation of Akt, and consequently the expression and production of HAS2 and HA is decreased. Akt and PI3K inhibitors also inhibit the production of HA by blocking HAS2 activation, whereas an inhibitor of NSMase2 has the reverse effect. This is the first time a connection between sphingolipid and glycosaminoglycan metabolic pathways has been made and involves regulation of the PI3K-PDK1-AKT-mTOR-p70S6K signaling pathway.

Because *fro*/*fro* is a mouse model of OI, our study may provide some clues showing the development of bone tissue. HA have diverse functions in skeletal biology including critical functions in bone and skeletal tissue development (60). The maturation of bone is associated with the reduction in HA and an increase in chondroitin sulfate (60), compared with increased HA production in *fro*/*fro* and OI. This suggested the potential role of HA in abnormal bone development. Although it is currently unclear how HA functions as a critical component of the musculoskeletal system, it clearly binds to specific membrane receptors such as TLR2 (24), affects cell adhesion and morphology, and induces less reactivity to mitogenic stimuli by transmembrane interactions with cytoskeleton. A more recent study (7) generated *fro*/*fro*-derived mice in which osteoblast-specific expression of *Smpd3* corrected bone abnormalities and increased long-chain ceramide levels in bone without affecting the cartilage phenotype. We used HPLC/MS/MS analysis to show that bone calvaria is rich in sphingolipids and that all species of ceramides are depleted in the *fro*/*fro* mouse. Although at the present time there is no human equivalent of the fragilis ossium syndrome caused by NSMase2 deletion, these findings suggest a potential novel pathway to understand the vital function of bioactive sphingolipids in generating and developing bone and connective tissue diseases. Furthermore, it would seem worthwhile to determine the expression level of *Smpd3* and to analyze the level of sphingolipid metabolites (*e.g.* ceramides and S1P) in human OI patients even if the primary mutation is not in the *Smpd3* gene.

Fig. 8 is a schematic explanation of the proposed connection between sphingolipid metabolism and glycosaminoglycan synthesis in *fro*/*fro* fibroblasts. The decreasing ceramide in *fro*/*fro* (NSMase2$^{-/-}$) fibroblasts inactivated PP2A and activated the PI3K/PDK1/Akt/mTOR/p70S6k signaling pathway, leading to up-regulation of HAS2 and hyaluronan synthesis. This is the first evidence from cell studies to support a mechanism to explain the formation of certain inherited OIs by regulation of HA through sphingolipid metabolites. We provide a mechanism for sphingolipid-induced, endogenous physiological regulation of HA, which may provide a clue to further investigating the etiology of certain noncollagen mutation-induced forms of OI.

Acknowledgments—All mass spectrometric analyses were performed at the University of Chicago Core facility. We thank Jonathan Goya for excellent technical assistance and Viswanathan Natarajan for technical advice. We thank Miriam Domowicz for helpful discussions regarding the analysis of hyaluronan and its mechanism of synthesis. The ASMase$^{-/-}$ mice were a generous gift from E. Schuchman (Mt. Sinai Medical Center, New York) and R. Wechselbaum (University of Chicago). Mouse fibroblast cultures were initiated by Sylvia Dawson and HPTLC was performed by John Kilkus.

REFERENCES

1. Sillence, D. O., Senn, A., and Danks, D. M. (1979) Genetic heterogeneity in osteogenesis imperfecta. *J. Med. Genet.* **16,** 101–116
2. Glorieux, F. H., Rauch, F., Plotkin, H., Ward, L., Travers, R., Roughley, P., Lalic, L., Glorieux, D. F., Fassier, F., and Bishop, N. J. (2000) Type V osteogenesis imperfecta. A new form of brittle bone disease. *J. Bone Miner. Res.* **15,** 1650–1658
3. Glorieux, F. H., Ward, L. M., Rauch, F., Lalic, L., Roughley, P. J., and Travers, R. (2002) Osteogenesis imperfecta type VI. A form of brittle bone disease with a mineralization defect. *J. Bone Miner. Res.* **17,** 30–38
4. Ward L. M., Rauch, F., Travers, R., Chabot, G., Azouz, E. M., Lalic, L., Roughley, P. J., and Glorieux, F. H. (2002) Osteogenesis imperfecta type VII. An autosomal recessive form of brittle bone disease. *Bone* **31,** 12–18

5. Aubin, I., Adams, C. P., Opsahl, S., Septier, D., Bishop, C. E., Auge, N., Salvayre, R., Negre-Salvayre, A., Goldberg, M., Guénet, J. L., and Poirier, C. (2005) A deletion in the gene encoding sphingomyelin phosphodiesterase 3 (*Smpd3*) results in osteogenesis and dentinogenesis imperfecta in the mouse. *Nat Genet.* **37,** 803–805
6. Stoffel, W., Jenke, B., Blöck, B., Zumbansen, M., and Koebke, J. (2005) Neutral sphingomyelinase 2 (*smpd3*) in the control of postnatal growth and development. *Proc. Natl. Acad. Sci. U.S.A.* **102,** 4554–4559
7. Khavandgar, Z., Poirier, C., Clarke, C. J., Li, J., Wang, N., McKee, M. D., Hannun, Y. A., and Murshed, M. (2011) A cell-autonomous requirement for neutral sphingomyelinase 2 in bone mineralization. *J. Cell Biol.* **194,** 277–289
8. Kolesnick, R., and Hannun, Y. A. (1999) Ceramide and apoptosis. *Trends Biochem. Sci.* **24,** 224–225; author reply 227
9. Wiesner, D. A., Kilkus, J. P., Gottschalk, A. R., Quintáns, J., and Dawson, G. (1997) Anti-immunoglobulin-induced apoptosis in WEHI 231 cells involves the slow formation of ceramide from sphingomyelin and is blocked by Bcl-xL. *J. Biol. Chem.* **272,** 9868–9876
10. Marchesini, N., Luberto, C., and Hannun, Y. A. (2003) Biochemical properties of mammalian neutral sphingomyelinase 2 and its role in sphingolipid metabolism. *J. Biol. Chem.* **278,** 13775–13783
11. Lee J. T., Xu J., Lee, J. M., Ku, G., Han, X., Yang, D. I., Chen, S., and Hsu, C. Y. (2004) Amyloid-β peptide induces oligodendrocyte death by activating the neutral sphingomyelinase-ceramide pathway. *J. Cell Biol.* **164,** 123–131
12. Testai, F. D., Landek, M. A., and Dawson, G. (2004) Regulation of sphingomyelinases in cells of the oligodendrocyte lineage. *J. Neurosci. Res.* **75,** 66–74
13. Chen, S., Lee, J. M., Zeng, C., Chen, H., Hsu, C. Y., and Xu, J. (2006) Amyloid β peptide increases DP5 expression via activation of neutral sphingomyelinase and JNK in oligodendrocytes. *J. Neurochem.* **97,** 631–640
14. Simons, K., and Ikonen, E. (1997) Functional rafts in cell membranes. *Nature* **387,** 569–572
15. Simons, K., and Toomre, D. (2000) Lipid rafts and signal transduction. *Nat. Rev. Mol. Cell Biol.* **1,** 31–39
16. Goswami R., Ahmed M., Kilkus J., Han T., Dawson SA, Dawson G. (2005) Differential regulation of ceramide in lipid-rich microdomains (rafts). Antagonistic role of palmitoyl:protein thioesterase and neutral sphingomyelinase 2. *J. Neurosci. Res.* **81,** 208–217
17. Tani, M., and Hannun, Y. (2007) Neutral sphingomyelinase 2 is palmitoylated on multiple cysteine residues. Role of palmitoylation in subcellular localization. *J. Biol. Chem.* **282,** 10047–10056
18. Maceyka, M., Payne, S. G., Milstien, S., and Spiegel, S. (2002) Sphingosine kinase, sphingosine-1-phosphate, and apoptosis. *Biochim. Biophys. Acta* **1585,** 193–201
19. Verheij, M., Bose, R., Lin, X. H., Yao, B., Jarvis, W. D., Grant, S., Birrer, M. J., Szabo, E., Zon, L. I., Kyriakis, J. M., Haimovitz-Friedman, A., Fuks, Z., and Kolesnick, R. N. (1996) Requirement for ceramide-initiated SAPK/JNK signalling in stress-induced apoptosis. *Nature* **380,** 75–79
20. Chalfant, C. E., Rathman, K., Pinkerman, R. L., Wood, R. E., Obeid, L. M., Ogretmen, B., and Hannun, Y. A. (2002) *De novo* ceramide regulates the alternative splicing of caspase 9 and Bcl-x in A549 lung adenocarcinoma cells. Dependence on protein phosphatase-1. *J. Biol. Chem.* **277,** 12587–12595
21. Gulbins, E., and Kolesnick, R. (2002) Acid sphingomyelinase-derived ceramide signaling in apoptosis. *Subcell. Biochem.* **36,** 229–244
22. Sawai, H., Domae, N., and Okazaki, T. (2005) Current status and perspectives in ceramide targeting molecular medicine. *Curr. Pharm. Des.* **11,** 2479–2487
23. Siskind, L. J., Kolesnick, R. N., and Colombini, M. (2006) Ceramide forms channels in mitochondrial outer membranes at physiologically relevant concentrations. *Mitochondrion* **6,** 118–125
24. Scheibner, K. A., Lutz, M. A., Boodoo, S., Fenton, M. J., Powell, J. D., and Horton, M. R. (2006) Hyaluronan fragments act as an endogenous danger signal by engaging TLR2. *J. Immunol.* **177,** 1272–1281
25. Turakainen, H., Larjava, H., Saarni, H., and Penttinen, R. (1980) Synthesis of hyaluronic acid and collagen in skin fibroblasts cultured from patients with osteogenesis imperfecta. *Biochem. Biophys. Acta* **628,** 338–397
26. Turakainen H. (1983) Altered glycosaminoglycan production in cultured osteogenesis-imperfecta skin fibroblasts. *Biochem. J.* **213,** 171–178
27. Kapoor, R., Bourier, S., and Prehm, P. (1983) Altered glycosaminoglycan production in cultured osteogenesis imperfecta skin fibroblasts. *FEBS Lett.* **2,** 171–178
28. Bastow, E. R., Byers, S., Golub, S. B., Clarkin, C. E., Pitsillides, A. A., and Fosang, A. J. (2008) Hyaluronan synthesis and degradation in cartilage and bone. *Cell. Mol. Life Sci.* **65,** 395–413
29. Tammi, R. H., Passi, A. G., Rilla, K., Karousou, E., Vigetti, D., Makkonen, K., and Tammi, M. I. (2011) Transcriptional and post-translational regulation of hyaluronan synthesis. *FEBS J.* **278,** 1419–1428
30. Kultti, A., Kärnä, R., Rilla, K., Nurminen, P., Koli, E., Makkonen, K. M., Si, J., Tammi, M. I., and Tammi, R. H. (2010) Methyl-β-cyclodextrin suppresses hyaluronan synthesis by down-regulation of hyaluronan synthase 2 through inhibition of Akt. *J. Biol. Chem.* **285,** 22901–22910
31. Weigel, P. H., and DeAngelis, P. L. (2007) Hyaluronan synthases, a decade-plus of novel glycosyltransferases. *J. Biol. Chem.* **282,** 36777–36781
32. Camenisch, T. D., Spicer, A. P., Brehm-Gibson, T., Biesterfeldt, J., Augustine, M. L., Calabro, A., Jr., Kubalak, S., Klewer, S. E., and McDonald, J. A. (2000) Disruption of hyaluronan synthase-2 abrogates normal cardiac morphogenesis and hyaluronan-mediated transformation of epithelium to mesenchyme. *J. Clin. Invest.* **106,** 349–360
33. Tlapak-Simmons, V. L., Medina, A. P., Baggenstoss, B. A., Nguyen, L., Baron, C. A., and Weigel, P. H. (2011) Clustered conserved cysteines in hyaluronan synthase mediate cooperative activation by Mg^{2+} ions and serve inhibitory effects of divalent cations. *J. Glycom. Lipidom.* S1–001
34. Tlapak-Simmons, V. L., Baggenstoss, B. A., Clyne, T., and Weigel, P. H. (1999) Purification and lipid dependence of the recombinant hyaluronan synthases from *Streptococcus pyogenes* and *Streptococcus equisimilis*. *J. Biol. Chem.* **274,** 4239–4245
35. Sakr, S. W., Potter-Perigo, S., Kinsella, M. G., Johnson, P. Y., Braun, K. R., Goueffic, Y., Rosenfeld, M. E., and Wight, T. N. (2008) Hyaluronan accumulation is elevated in cultures of low density lipoprotein receptor-deficient cells and is altered by manipulation of cell cholesterol content. *J. Biol. Chem.* **283,** 36195–36204
36. Kilkus, J., Goswami, R., Testai, F. D., and Dawson, G. (2003) Ceramide in rafts (detergent-insoluble fraction) mediates cell death in neurotumor cell lines. *J Neurosci Res* **72,** 65–75
37. Bligh, E., and Dyer, W. J. (1959) A rapid method of tatal lipid extraction and purification. *Can. J. Biochem. Physiol.* **37,** 911–917
38. Vaskovsky, V. E., Kostetsky, E. Y., and Vasendin, I. M. (1975) A universal reagent for phospholipid analysis. *J. Chromatogr.* **114,** 129–141
39. Berdyshev, E. V., Gorshkova, I. A., Usatyuk, P., Zhao, Y., Saatian, B., Hubbard, W., Natarajan, V. (2006) De novo biosynthesis of dihydrosphingosine 1-phosphate by sphingosine kinase 1 in mammalian cells. *Cell. Signal.* **18,** 1779–1792
40. Qin, J., Berdyshev, E., Goya, J., Natarajan, V., and Dawson, G. (2010) Neurons and oligodendrocytes recycle sphingosine 1-phosphate to ceramide. Significance for apoptosis and multiple sclerosis. *J. Biol. Chem.* **285,** 14134–14143
41. Pewzner-Jung, Y., Ben-Dor, S., and Futerman, A. H. (2006) When do Lasses (longevity assurance genes) become CerS (ceramide synthases)? Insights into the regulation of ceramide synthesis. *J. Biol. Chem.* **281,** 25001–25005
42. Horinouchi, K., Erlich, S., Perl, D. P., Ferlinz, K., Bisgaier, C. L., Sandhoff, K., Desnick, R. J., Stewart, C. L., and Schuchman, E. H. (1995) Acid sphingomyelinase deficient mice. A model of types A and B Niemann-Pick disease. *Nat. Genet.* **10,** 288–293
43. Otterbach, B., and Stoffel, W. (1995) Acid sphingomyelinase-deficient mice mimic the neurovisceral form of human lysosomal storage disease (Niemann-Pick disease). *Cell* **81,** 1053–1061
44. Wolff, R. A., Dobrowsky, R. T., Bielawska, A., Obeid, L. M., and Hannun, Y. A. (1994) Role of ceramide-activated protein phosphatase in ceramide-mediated signal transduction. *J. Biol. Chem.* **269,** 19605–19609
45. Goswami, R., Kilkus, J., Dawson, S. A., and Dawson, G. (1999) Overexpression of Akt (protein kinase B) confers protection against apoptosis and prevents formation of ceramide in response to pro-apoptotic stimuli. *J. Neurosci. Res.* **57,** 884–893

46. Zhou, H., Summers, S. A., Birnbaum, M. J., and Pittman, R. N. (1998) Inhibition of Akt kinase by cell-permeable ceramide and its implications for ceramide-induced apoptosis. *J. Biol. Chem.* **273,** 16568–16575
47. Osawa, Y., Uchinami, H., Bielawski, J., Schwabe, R. F., Hannun, Y. A., and Brenner, D. A. (2005) Roles for C_{16}-ceramide and sphingosine 1-phosphate in regulating hepatocyte apoptosis in response to tumor necrosis factor-α. *J. Biol. Chem.* **280,** 27879–27887
48. Banno, Y., Takuwa, Y., Akao, Y., Okamoto, H., Osawa, Y., Naganawa, T., Nakashima, S., Suh, P. G., and Nozawa, Y. (2001) Involvement of phospholipase D in sphingosine 1-phosphate-induced activation of phosphatidylinositol 3-kinase and Akt in Chinese hamster ovary cells overexpressing EDG3. *J. Biol. Chem.* **276,** 35622–35628
49. Moscatelli, D., and Rubin, H. (1975) Increased hyaluronic acid production on stimulation of DNA synthesis in chick embryo fibroblasts. *Nature* **254,** 65–66
50. Matuoka, K., Mitsui, Y., and Murota, S. I. (1985) Growth coupled changes in glucosaminoglycans (heparan sulfate and hyaluronic acid) in normal and transformed human fibroblasts. *Cell Biol. Int. Rep.* **9,** 577–586
51. Yoneda, M., Shimizu, S., Nishi, Y., Yamagata, M., Suzuki, S., and Kimata, K. (1988) Hyaluronic acid-dependent change in the extracellular matrix of mouse dermal fibroblasts that is conducive to cell proliferation. *J. Cell Sci.* **90,** 275–286
52. West, D. C., and Kumar, S. (1989) The effect of hyaluronate and its oligosaccharides on endothelial cell proliferation and monolayer integrity. *Exp. Cell Res.* **183,** 179–196
53. Galvan, C., Camoletto, P. G., Cristofani, F., Van Veldhoven, P. P., and Ledesma, M. D. (2008) Anomalous surface distribution of glycosyl phosphatidyl inositol-anchored proteins in neurons lacking acid sphingomyelinase. *Mol. Biol. Cell* **19,** 509–522
54. Jenkins, R. W., Idkowiak-Baldys, J., Simbari, F., Canals, D., Roddy, P., Riner, C. D., Clarke, C. J., and Hannun, Y. A. (2011) A novel mechanism of lysosomal acid sphingomyelinase maturation. Requirement for carboxyl-terminal proteolytic processing. *J. Biol. Chem.* **286,** 3777–3788
55. Hannun, Y. A., and Obeid, L. M. (2008) Principles of bioactive lipid signaling. Lessons from sphingolipids. *Nat. Rev. Mol. Cell Biol.* **9,** 139–150
56. Osaki, M., Oshimura, M., and Ito, H. (2004) PI3K-Akt pathway. Its functions and alterations in human cancer. *Apoptosis* **9,** 667–676
57. Goswami, R., Singh, D., Phillips, G., Kilkus, J., and Dawson, G. (2005) Ceramide regulation of the tumor suppressor phosphatase PTEN in rafts isolated from neurotumor cell lines. *J. Neurosci. Res.* **81,** 541–550
58. Vigetti, D., Genasetti, A., Karousou, E., Viola, M., Moretto, P., Clerici, M., Deleonibus, S., De Luca, G., Hascall, V. C., and Passi, A. (2010) Proinflammatory cytokines induce hyaluronan synthesis and monocyte adhesion in human endothelial cells through hyaluronan synthase 2 (HAS2) and the nuclear factor-κB (NF-κB) pathway. *J. Biol. Chem.* **285,** 24639–24645
59. Spiegel, S., and Milstien, S. (2003) Sphingosine-1-phosphate. An enigmatic signalling lipid. *Nat. Rev. Mol. Cell Biol.* **4,** 397–407
60. Hall, B. K., and Miyake, T. (1995) Divide, accumulate, differentiate. Cell condensation in skeletal development revisited. *Int. J. Dev. Biol.* **3,** 881–893